

Lagrangian Drifter Dispersion in the Southwestern Atlantic Ocean

Stefano Berti, Francisco Alves dos Santos, Guglielmo Lacorata, Angelo Vulpiani

▶ **To cite this version:**

Stefano Berti, Francisco Alves dos Santos, Guglielmo Lacorata, Angelo Vulpiani. Lagrangian Drifter Dispersion in the Southwestern Atlantic Ocean. Journal of Physical Oceanography, 2011, 41 (9), pp.1659-1672. 10.1175/2011jpo4541.1 . hal-01119197

HAL Id: hal-01119197
https://hal.science/hal-01119197

Submitted on 22 Feb 2015

HAL is a multi-disciplinary open access archive for the deposit and dissemination of scientific research documents, whether they are published or not. The documents may come from teaching and research institutions in France or abroad, or from public or private research centers.

L'archive ouverte pluridisciplinaire **HAL**, est destinée au dépôt et à la diffusion de documents scientifiques de niveau recherche, publiés ou non, émanant des établissements d'enseignement et de recherche français ou étrangers, des laboratoires publics ou privés.

Lagrangian Drifter Dispersion in the Southwestern Atlantic Ocean

STEFANO BERTI

Laboratoire Interdisciplinaire de Physique, Grenoble, and Laboratoire de Météorologie Dynamique, Paris, France

FRANCISCO ALVES DOS SANTOS

PROOCEANO Serviço Oceanográfico, Rio de Janeiro, Brazil

GUGLIELMO LACORATA

Institute of Atmospheric and Climate Sciences, National Research Council, Lecce, Italy

ANGELO VULPIANI

Department of Physics, CNR-ISC and INFN, Sapienza University of Rome, Rome, Italy

(Manuscript received 2 August 2010, in final form 24 February 2011)

ABSTRACT

In the framework of Monitoring by Ocean Drifters (MONDO) project, a set of Lagrangian drifters were released in proximity of the Brazil Current, the western branch of the subtropical gyre in the South Atlantic Ocean. The experimental strategy of deploying part of the buoys in clusters offers the opportunity to examine relative dispersion on a wide range of scales. Adopting a dynamical systems approach, the authors focus their attention on scale-dependent indicators, like the finite-scale Lyapunov exponent (FSLE) and the finite-scale (mean square) relative velocity (FSRV) between two drifters as a function of their separation and compare them with classic time-dependent statistical quantities like the mean-square relative displacement between two drifters and the effective diffusivity as functions of the time lag from the release. The authors find that, dependently on the given observable, the quasigeostrophic turbulence scenario is overall compatible with their data analysis, with discrepancies from the expected behavior of 2D turbulent trajectories likely to be ascribed to the nonstationary and nonhomogeneous characteristics of the flow, as well as to possible ageostrophic effects. Submesoscale features of $\sim O(1)$ km are considered to play a role, to some extent, in determining the properties of relative dispersion as well as the shape of the energy spectrum. The authors also present numerical simulations of an ocean general circulation model (OGCM) of the South Atlantic and discuss the comparison between experimental and model data about mesoscale dispersion.

1. Introduction

Detailed investigation of geophysical flows involves experimental campaigns in which buoys, in the ocean, or balloons, in the atmosphere, are released to collect Lagrangian data against which theories and models can be tested. Questions concerning oil spill fate, fish larvae distribution, or search and rescue operations are only a few examples that make the study of advection and diffusion properties not only a challenging scientific task but also a matter of general interest.

In past years, an amount of Lagrangian data about the South Atlantic Ocean (SAO) was collected thanks to the First Global Atmospheric Research Program (GARP) Global Experiment (FGGE) drifters, released following the major shipping lines; the Southern Ocean Studies (SOS) drifters, deployed in the Brazil–Malvinas Confluence (BMC); and the Programa Nacional de Bóias (PNBOIA) drifters [Brazilian contribution to the Global Oceans Observing System (GOOS)], released in the Southeastern Brazilian Bight (SBB). These data allowed estimates of eddy kinetic energy (EKE), integral time scales, and diffusivities (Piola et al. 1987; Figueroa and

Corresponding author address: Guglielmo Lacorata, Institute of Atmospheric and Climate Sciences, National Research Council, Str. Lecce-Monteroni, I-73100 Lecce, Italy.
E-mail: g.lacorata@isac.cnr.it

DOI: 10.1175/2011JPO4541.1

© 2011 American Meteorological Society

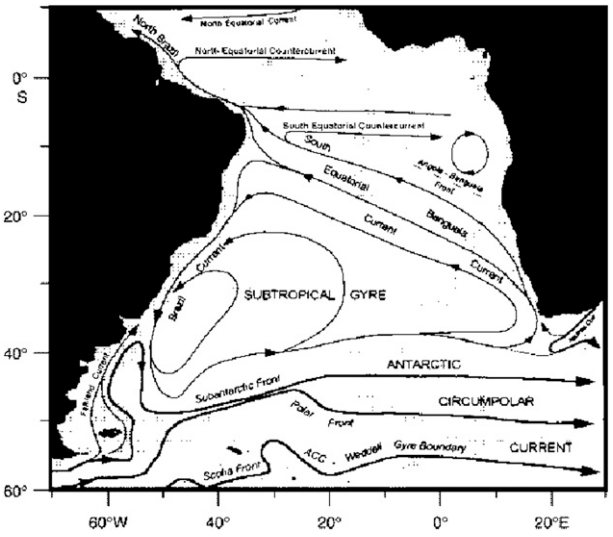


FIG. 1. Large-scale surface circulation in the SAO (courtesy of Integrated Ocean Drilling Program; available online at http://www.iodp.org/).

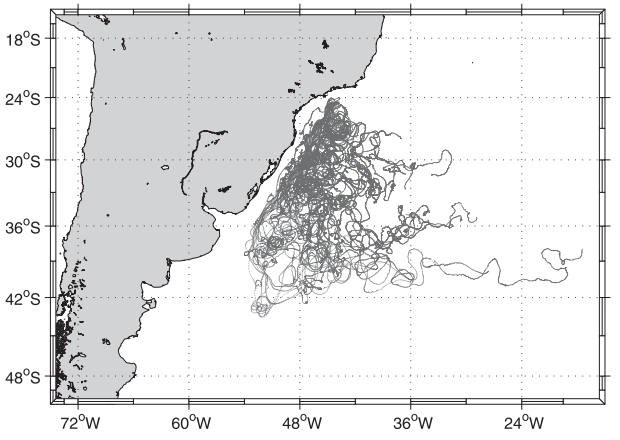


FIG. 2. Overall view of the trajectories of MONDO drifters.

Olson 1989; Schäfer and Krauss 1995). Despite the relatively uniform coverage, the boundary currents resulted poorly populated by buoys; furthermore, all previous studies about drifters in the South Atlantic have concerned one-particle statistics only. In this regard, in the framework of the Monitoring by Ocean Drifters (MONDO) project, a recent Lagrangian experiment, consisting in the release of a set of 39 World Ocean Circulation Experiment (WOCE) Surface Velocity Programme (SVP) drifters, was planned in relationship with an oil drilling operation in proximity of the coast of Brazil, around (24°S, 44°E). Part of the drifters was deployed in five-element clusters, some of them with initial drifter separations smaller than 1 km. This set of satellite-tracked Lagrangian trajectories offers now the opportunity to revisit advective and diffusive properties characterizing the current systems explored by the drifters. From the analysis of trajectory pair dispersion, we can extract, in principle, information about the dominant physical mechanism acting at a certain scale of motion (e.g., chaotic advection, turbulence, diffusion). A thorough description of the oceanography of the South Atlantic Ocean, particularly of the main circulation patterns and of the mass transport properties, can be found in Peterson and Stramma (1991), Campos et al. (1995), and Stramma and England (1999). The major feature characterizing the central region of the SAO is the large anticyclonic (anticlockwise) circulation known as the subtropical gyre (SG). Other relevant surface current systems are the South Equatorial Current (SEC), Brazil Current (BC), Malvinas Current (MC), South Atlantic Current (SAC), and Benguela Current (BgC), as shown in Fig. 1.

In the quasigeostrophic (QG) approximation, valid for relative vorticities much smaller than the ambient vorticity because of the earth's rotation, some theoretical arguments would predict that, from the scale of the forcing at which eddies are efficiently generated by instability (e.g., the Rossby radius of deformation), both a downscale enstrophy cascade and an upscale energy cascade take place, corresponding to energy spectra $E(k) \sim k^{-3}$ and $E(k) \sim k^{-5/3}$, respectively (Kraichnan 1967; Charney 1971). From a relative dispersion perspective, in the forward cascade range, the mean-square relative displacement between two trajectories grows exponentially fast in time (Lin 1972), whereas, in the inverse cascade range, it follows the $\sim t^3$ power law (Obhukov 1941; Batchelor 1950). Possible deviations from this ideal picture may reasonably come from the nonhomogeneous and nonstationary characteristics of the velocity field: for example, in the case of boundary currents, as well as from ageostrophic effects. At this regard, one presently debated issue is the role of submesoscale vortices (McWilliams 1985) [velocity field features of size $\sim O(1)$ km] in determining the shape of the energy spectrum at intermediate scales between the Rossby deformation radius [in the ocean typically $\sim$(10–50) km] and the dissipative scales (much smaller than 1 km). A thorough discussion about submesoscale processes and dynamics can be found in Thomas et al. (2008). Recent high-resolution 3D simulations of upper-layer turbulence (Capet et al. 2008a,b; Klein et al. 2008) have shown that the direct cascade energy spectrum flattens from k^{-3} to k^{-2} for order $O(1)$ Rossby number $R_o = U/fL$, where U is the typical velocity difference on a characteristic length L of the flow and $f \simeq 10^{-4}\ \mathrm{s}^{-1}$ is the Coriolis parameter.

Our main purpose is to exploit the MONDO drifter trajectories, shown in Fig. 2, to examine relative dispersion

by means of several indicators and discuss the consistency of our data analysis in comparison with classical turbulence theory predictions, model simulations and previous drifter studies available for different regions of the ocean. This paper is organized as follows: in section 2, we recall the definitions of the major indicators of the Lagrangian dispersion process; in section 3, we give a description of the MONDO drifter Lagrangian data; in section 4, the outcome of the data analysis is presented; in section 5, we report the analysis of the ocean model Lagrangian simulations in comparison with the observative data; and, in section 6, we outline and discuss the main results we have obtained in the present work.

2. Lagrangian dispersion indicators

a. One-particle statistics

Let $\mathbf{r} = (x, y, z)$ be the position vector of a Lagrangian particle, in a 3D space, evolving according to the equation $d\mathbf{r}/dt = \mathbf{U}(x, y, z, t)$, where $\mathbf{U}(x, y, z, t)$ is a 3D Eulerian velocity field, and let us indicate with $\mathbf{v}(t)$ the Lagrangian velocity along the trajectory $\mathbf{r}(t)$. Let us imagine, then, a large ensemble of $N \gg 1$ Lagrangian particles, passively advected by the given velocity field, and refer, for every statistically averaged quantity, to the mean over the ensemble.

The autocorrelation function of a Lagrangian velocity component v can be defined, for $t_1 \geq t_0$, as

$$C(t_1, t_0) = [\langle v(t_1)v(t_0)\rangle - \langle v(t_0)\rangle^2]/[\langle v(t_0)^2\rangle - \langle v(t_0)^2\rangle]. \tag{1}$$

In case of stationary statistics, $C(t_1, t_0)$ depends only on the time lag $t = t_1 - t_0$. The integral Lagrangian time τ_L is the time scale after which the autocorrelation has nearly relaxed to zero. Typically, τ_L can be estimated as the time of the first zero crossing of $C(t_1, t_0)$ or alternatively as the time after which $|C(t_1, t_0)|$ remains smaller than a given threshold.

Absolute dispersion can be defined as the variance of the particle displacement relatively to the mean position at time t,

$$\langle A^2(t)\rangle = \langle [\mathbf{r}(t) - \mathbf{r}(0)]^2\rangle - \langle [\mathbf{r}(t) - \mathbf{r}(0)]\rangle^2. \tag{2}$$

In the limit of very small times, absolute dispersion is expected to behave as follows:

$$\langle A(t)^2\rangle \simeq \sigma_L^2 t^2, \quad \text{for} \quad t \ll \tau_L, \tag{3}$$

where τ_L is the Lagrangian autocorrelation time and σ_L^2 is the total Lagrangian velocity variance. The ballistic regime (3) lasts as long as the trajectories save some memory of their initial conditions. In the opposite limit of very large times, when the autocorrelations have relaxed to zero and the memory of the initial conditions is lost, we have

$$\langle A(t)^2\rangle \simeq 2Kt, \quad \text{for} \quad t \gg \tau_L, \tag{4}$$

where K is the absolute diffusion coefficient (Taylor 1921).

Although single-particle statistics give information about the advective transport, mostly because of the largest and most energetic scales of motion, two (or more) particle statistics give information about the physical mechanisms acting at any scale of motion, compatibly with the available resolution.

b. Two-particle statistics

Let us indicate with $R(t) = \|\mathbf{r}^{(1)}(t) - \mathbf{r}^{(2)}(t)\|$ the distance between two trajectories at time t. Relative dispersion is defined as the second-order moment of $R(t)$,

$$\langle R^2(t)\rangle = \langle \|\mathbf{r}^{(1)}(t) - \mathbf{r}^{(2)}(t)\|^2\rangle, \tag{5}$$

where the average is over all the available trajectory pairs $(\mathbf{r}^{(1)}, \mathbf{r}^{(2)})$.

In the small-scale range, the velocity field between two sufficiently close trajectories is reasonably assumed to vary smoothly. This means that, in nonlinear flows, the particle pair separation typically evolves following an exponential law,

$$\langle R^2(t)\rangle \sim e^{L(2)t}, \tag{6}$$

where, from the theory of dynamical systems, $L(2)$ is the generalized Lyapunov exponent of order 2 (Bohr et al. 1998). When fluctuations of the finite-time exponential growth rate around its mean value are weak, one has $L(2) \simeq 2\lambda_L$, where λ_L is the (Lagrangian) maximum Lyapunov exponent (MLE; Boffetta et al. 2000). Notice that, for ergodic trajectory evolutions, the Lyapunov exponents do not depend on the initial conditions. If $\lambda_L > 0$ (except for a set of zero probability measure), we speak of Lagrangian chaos. The chaotic regime holds as long as the trajectory separation remains sufficiently smaller than the characteristic scales of motion.

In the opposite limit of large particle separations, when two trajectories are sufficiently distant from each other to be considered uncorrelated, the mean-square relative displacement behaves as

$$\langle R^2(t)\rangle \simeq 4K_E t, \quad \text{for} \quad t \to \infty, \tag{7}$$

where we indicate with K_E the asymptotic eddy-diffusion coefficient (Richardson 1926).

At any time t, the diffusivity $K(t)$ can be defined as

$$K(t) = \frac{1}{4}\left\langle \frac{dR^2}{dt}(t) \right\rangle = \frac{1}{2}\left\langle R(t)\frac{dR}{dt}(t) \right\rangle, \tag{8}$$

with $K(t) \to K_E$ for $t \to \infty$.

If the velocity field is characterized by several scales of motion, relative dispersion in the intermediate range (i.e., between the smallest and the largest characteristic length) depends on the properties of local velocity differences (i.e., the mean gradients on finite scale). For instance, in 3D fully developed turbulence (Frisch 1995), relative dispersion follows the so-called Richardson's law,

$$\langle R^2(t) \rangle \sim t^{\gamma}, \tag{9}$$

with $\gamma = 3$, as long as the trajectory separation lies in the inertial range of the energy cascade (Richardson 1926) from large to small scales. It is worth to remark that Richardson's law also holds in the inverse cascade range (from small to large scales) of 2D turbulence because, in that case as well, the energy spectrum follows Kolmogorov's $k^{-5/3}$ scaling, exactly as in the inertial range of 3D turbulence (Kraichnan 1967). Any power law of the type (9) for $\langle R^2(t) \rangle$ with $\gamma > 1$ is known as superdiffusion.

c. Scale-dependent indicators

The finite-scale Lyapunov exponent (FSLE) has been formerly introduced as the generalization of the MLE λ for noninfinitesimal perturbations (Aurell et al. 1996). If δ is the size of the perturbation on a trajectory in the phase space of a system and $\langle \tau(\delta) \rangle$ is the phase space averaged time that δ takes to be amplified by a factor $\rho > 1$, then the FSLE is defined as

$$\lambda(\delta) = \frac{1}{\langle \tau(\delta) \rangle} \ln \rho. \tag{10}$$

The quantity $\tau(\delta)$ is the exit time of the perturbation size from the scale δ, and it is defined as the first arrival time to the scale $\rho\delta$ with $\rho \sim O(1)$. The computation of the expectation value of the growth rate at a fixed scale, which justifies the definition (10), is described in Boffetta et al. (2000). As far as Lagrangian dynamics are concerned, the evolution equations of the Lagrangian trajectories form a dynamical system whose phase space is the physical space spanned by the trajectories. In this context, the analysis of relative dispersion can be treated as a problem of finite-size perturbation evolution, with scale-dependent growth rate measured by the FSLE. The first who had the idea to measure the relative dispersion, or equivalently the diffusivity, as a function of the trajectory separation was Richardson (1926). The FSLE is fundamentally based on the same principle. Recently, the use of fixed-time and fixed-scale averaged indicators of relative dispersion in various contexts, from dynamical systems to observative data in ocean and atmosphere, have been reviewed and discussed in several works (Artale et al. 1997; Boffetta et al. 2000; Lacorata et al. 2001, 2004; LaCasce and Ohlmann 2003; LaCasce 2008). By a dimensional argument, if relative dispersion follows a $\langle R^2(t) \rangle \sim t^{2/\beta}$ scaling law, then the FSLE is expected to scale as $\lambda(\delta) \sim \delta^{-\beta}$. For example, in the case of standard diffusion, we expect $\beta = 2$; in Richardson's superdiffusion, $\beta = 2/3$; and, in ballistic or shear dispersion, we have $\beta = 1$. Chaotic advection means exponential separation between trajectories. In terms of FSLE, this amounts to a scale-independent $\lambda(\delta) =$ constant: that is, $\beta \to 0$. In the limit of infinitesimal separation, the FSLE is nothing but the MLE: that is, $\lambda(\delta) \simeq \lambda_L$ (Aurell et al. 1996). Under these conditions, relative dispersion is said to be a nonlocal process, because it is determined by velocity field structures with a characteristic scale much larger than the particle separation. On the contrary, when the growth of the distance between two particles is mainly driven by velocity field structures of the same scale as the particle separation, relative dispersion is said to be a local process. The superdiffusive processes occurring in 2D and 3D turbulence are phenomena of this type.

An indicator related to the FSLE is the mean-square velocity difference between two trajectories as function of their separation. Indicating with $\mathbf{r}^{(1)}$, $\mathbf{r}^{(2)}$, $\mathbf{v}^{(1)}$, and $\mathbf{v}^{(2)}$ the positions and the Lagrangian velocities of two particles 1 and 2 at a given time, respectively, we define the finite-scale relative velocity (FSRV) at scale δ,

$$\langle [\Delta V(\delta)]^2 \rangle = \langle [\mathbf{v}^{(1)} - \mathbf{v}^{(2)}]^2 \rangle, \tag{11}$$

where the average is over all trajectory pairs fulfilling the condition $R(t) = \|\mathbf{r}^{(1)}(t) - \mathbf{r}^{(2)}(t)\| = \delta$ at some time t. From the FSRV, a scale-dependent diffusivity can be formed as $K(\delta) = (1/2)\delta\langle [\Delta V(\delta)]^2 \rangle^{1/2}$ and compared to the classical time-dependent diffusivity $K(t)$ defined in (8).

We would like to end this section with a remark. It is physically reasonable to assume that, for statistically homogeneous flows, the behavior of the relative dispersion changes in correspondence of certain characteristic lengths of the system, rather than after certain time intervals. The major shortcoming when measuring the mean-square relative displacement at fixed time consists in averaging together particle pairs that may have very different separations: that is, may belong to very different dispersion regimes. On the contrary, the

mean dispersion rate at fixed scale or other scale-dependent related quantities generally have the benefit of being weakly affected by possible overlap effects. This is of particular relevance because the presence of scaling laws in the pre-asymptotic regime raises questions about the characteristics (e.g., the kinetic energy spectrum) of the underlying velocity field.

3. Dataset and local oceanography

The MONDO project is a campaign planned by PROOCEANO for Eni Oil do Brasil to provide unrestricted access to oceanographic data and subsidize not only the company's operational goals but also the scientific community. The Lagrangian experiment consisted in the deployment of 39 WOCE SVP drifters (Sybrandy and Niiler 1991) in the surroundings of an oil drilling operation (24°24′50″S, 43°46′22″W) in proximity of the BC. The drifters are of the holey-sock type, composed by a surface floater, a tether and a submerged drogue, following the design criteria proposed by Sybrandy and Niiler (1991). The drogue length is 6.44 m, centered at 15 m deep, to represent the first 20-m current information. The drifters are equipped with a GPS device and iridium transmission, providing a positioning accuracy of 7 m and an acquiring rate of 3 h. From the 39 drifters, 14 were deployed individually in a 3-day frequency and 25 were deployed in clusters of 5, every 12 days. Justification for the 3-day frequency deployment is based on the 6.5-day energy peak in the wind variability in the region (Stech and Lorenzetti 1992). Data used in this study comprehend the period within 21 September 2007–14 November 2008 and passed the quality control proposed by Hansen and Poulain (1996) in the Global Drifter Program (GDP) database. High-frequency components have been removed by applying a Blackman low-pass filter with a window of 15 points (45 h).

The domain explored by the MONDO project drifters mainly corresponds to that of the BC and to the area where the southward-flowing BC meets the northward-flowing MC, forming the BMC, which results in an eastward current feeding the SAC. BC is a warm western boundary current, flowing southward and meandering over the 200-m isobath (Peterson and Stramma 1991; Lima et al. 1996). As reported by de Castro et al. (2006) and Garfield (1990), the velocities inside the BC have values between 25 and 80 cm s^{-1}. BC flux increases with latitude (Assireu 2003; Müller et al. 1998; Gordon and Greengrove 1986) and veers toward the east when meeting the colder Malvinas Current around 40°S. The BMC is a highly energetic zone with strong thermal gradient and great variability, playing an important role in weather and climate of South America (Legeckis and Gordon 1982; Pezzi et al. 2005; Piola et al. 2008). Both BC and BMC show intense mesoscale activity with eddies detaching from both sides of the flow. Lentini et al. (2002) used satellite-derived sea surface temperature (SST) to estimate an average of 7 rings per year, with lifetimes ranging from 11 to 95 days with major and minor radii of 126 ± 50 km and 65 ± 22 km, respectively. Assireu (2003) estimates a diffusion coefficient between 6×10^6 and 9.1×10^7 cm^2 s^{-1}; a Lagrangian time scale between 1 and 5 days; and a characteristic (Eulerian) length scale varying from 19 to 42 km, which agrees with the meridional variation of the first internal Rossby radius of deformation in the region (Houry et al. 1987). Studies addressing the energetics in BC and BMC flows report great spatial and temporal variability (see, e.g., Assireu et al. 2003; Piola et al. 1987; Stevenson 1996) with EKE varying from 200 to 1200 cm^2 s^{-2} and representing 70%–90% of the total kinetic energy (TKE). Recently, Oliveira et al. (2009) extended the analysis made by Piola et al. (1987) and suggested that EKE is usually lower than the mean kinetic energy (MKE) in the BC and always greater in the BMC.

4. Data analysis

a. Single-particle statistics

From a pre-analysis, we eliminated two drifters that very soon lost their drogue, so the set of active drifters is reduced to 37 units. The Lagrangian velocity statistics, reconstructed along the drifter trajectories by means of a finite-difference scheme, provides standard deviations, in the zonal and meridional directions, on the order of $\simeq$25 cm s^{-1}, compatible with estimates obtained from other observative data available for the same ocean region (Figueroa and Olson 1989; Schäfer and Krauss 1995).

The drifters initially tend to move southward, driven by the BC; then they are nearly stopped by the BMC; and last they tend to be transported eastward by the SAC. The time evolution of the drifter mean position coordinates in longitude and latitude is shown in Fig. 3. During the first phase of dispersion, the mean meridional displacement grows almost linearly southward (BC), whereas the mean zonal displacement is almost constant; after about 120 days from the release time, the mean meridional displacement tends to saturate (BMC), whereas the mean zonal displacement tends to grow almost linearly eastward (SAC). Given the differences between BC, BMC, and SAC in terms of energy and circulation patterns and, in general, between the boundary of the subtropical gyre and its interior, the drifters do

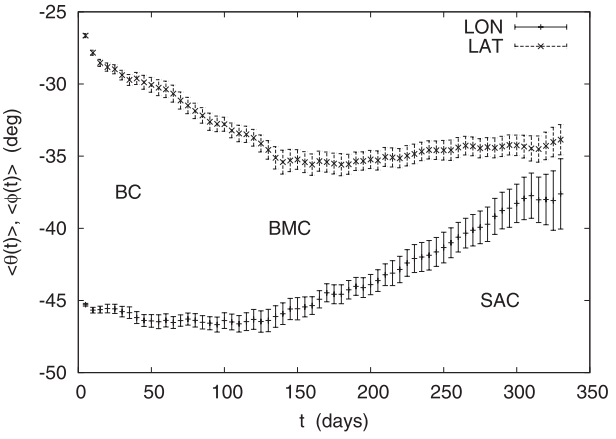


FIG. 3. Mass center coordinates in longitude $\langle\theta\rangle$ and latitude $\langle\phi\rangle$, averaged over all drifters, as function of the time lag since the release. The time sampling is $\Delta t = 1/8$ day. Error bars are the standard deviations of the mean values.

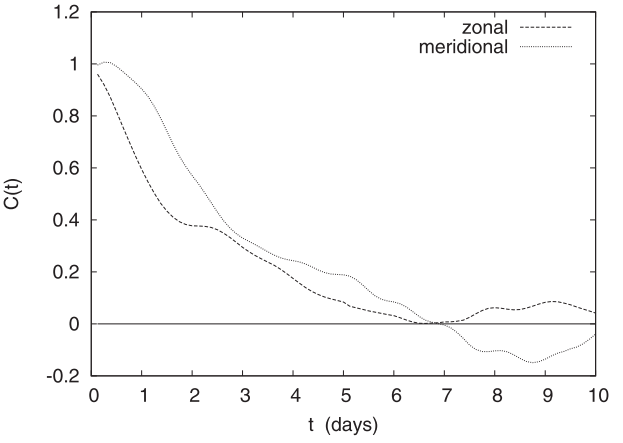


FIG. 4. Lagrangian velocity autocorrelation function for zonal and meridional components. The time sampling is $\Delta t = 1/8$ day.

not sample a statistically homogeneous and stationary domain. To evaluate the Lagrangian autocorrelations, we divide the trajectory lifetime into time windows of 10-day widths. Then, we compute (1), where mean and variance of the Lagrangian velocity components are recalculated for each window, and then we take the average, for a fixed time lag $t = t_1 - t_0$, over all the windows for all trajectories. The resulting functions are plotted in Fig. 4. We notice that, because most of the statistics regards trajectory segments within or near the BC, the motion is slightly more autocorrelated in the meridional direction than in the zonal direction. However, the order of the integral time scale is the same for both components. Without discussing the various estimates that can be evaluated using different criteria, we identify the two integral time scales around a value $\tau_L \simeq 5$ days, with a difference between zonal and meridional components of $O(1)$ days. This implies that, for time lags significantly larger than τ_L, the Lagrangian velocities along a trajectory become practically uncorrelated.

Absolute dispersion (i.e., the mean-square fluctuation around the mean position) for zonal and meridional coordinates is reported in Fig. 5. In the present work, we are not interested in reproducing estimates of small-scale diffusivity, obtained by reconstructing a mean velocity field, in general not spatially uniform, and calculating the turbulent components from the difference between the drifter local velocities and the local mean field. Wherever we speak of diffusion coefficients, referring to (2) or (5), we mean the effective diffusion coefficients of $\sim O(UL)$, where L and U are determined by the characteristic size and rotation velocity of the largest eddies, respectively. Absolute dispersion, being dominated by the large-scale features of the velocity field, reflects the anisotropy of the currents encountered by the drifters. The ballistic dispersion $\sim t^2$ scaling is plotted as reference for autocorrelated motions on time lags smaller than 10 days. The diffusion $\sim t$ scaling is a good approximation for meridional dispersion on time lags within 10–60 days, but it is not good for zonal dispersion on any time lag. After about 60 days, meridional dispersion tends to saturate, whereas zonal dispersion starts growing again as $\sim t^2$, likely because on those time lags, on average, the drifters have reached the BMC, have stopped their southward meridional run along the BC, and start moving eastward along the SAC, the natural consequence of which is the saturation of the meridional component and a second ballistic (or shear) regime for the zonal component.

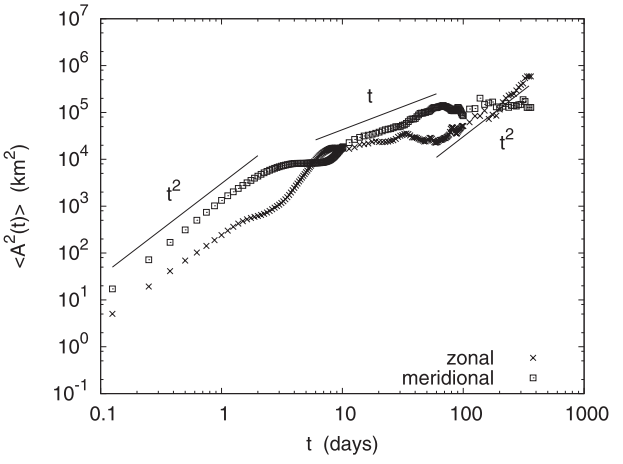


FIG. 5. Mean-square drifter displacement from the mass center position $\langle A^2(t)\rangle$ in zonal and meridional components. The time sampling is $\Delta t = 1/8$ day.

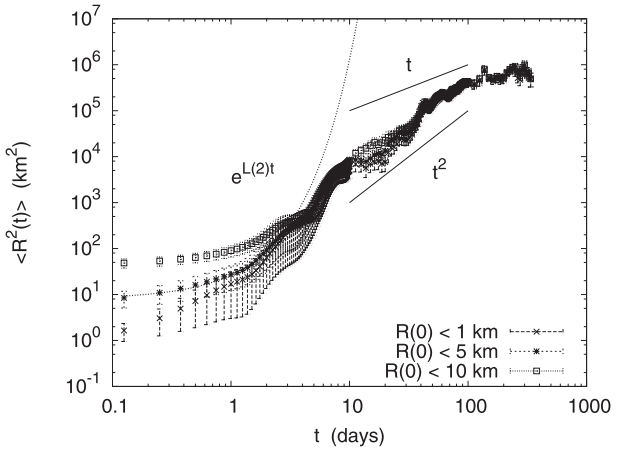


FIG. 6. Drifter relative dispersion $\langle R^2(t)\rangle$ for initial separations $R(0) \leq 1$, ≤ 5, and ≤ 10 km. The quantity $L(2) \simeq 1.2$ day^{-1} corresponds to $\lambda_L \simeq 0.6$ day^{-1}. The time sampling is $\Delta t = 1/8$ day. Error bars are the standard deviations of the mean values.

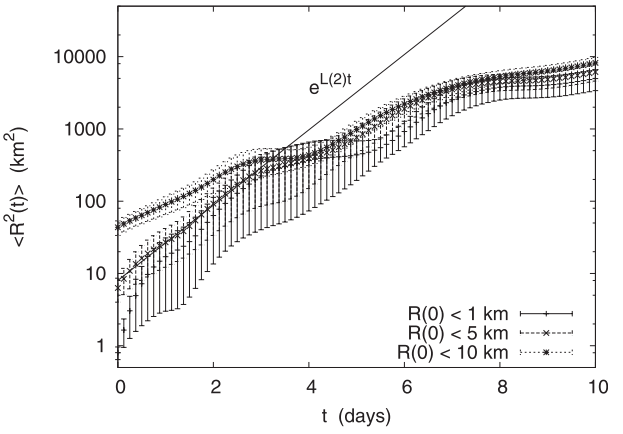


FIG. 7. Early regime of drifter relative dispersion $\langle R^2(t)\rangle$ for initial separations $R(0) \leq 1$, ≤ 5, and ≤ 10 km with $L(2) \simeq 2\lambda_L \simeq 1.2$ day^{-1}. The time sampling is $\Delta t = 1/8$ day. Error bars are the standard deviations of the mean values.

b. *Two-particle statistics*

Relative dispersion for three different initial separations is shown in Fig. 6. Distances between two points on the ocean surface are calculated as great circle arcs, according to the spherical geometry standard approximation. A way to increase relative dispersion statistics is to measure (5) also for so-called chance pairs: that is, particle pairs that may be initially very distant from each other but that, following the flow, happen to get sufficiently close to each other at some later time after their release, in some random point of the domain (LaCasce 2008). The maximum number of pairs counted in the statistics depends on the initial threshold: 24 pairs for $R(0) \leq 1$ km, 30 pairs for $R(0) \leq 5$ km, and 39 pairs for $R(0) \leq 10$ km. The dependence of $\langle R^2(t)\rangle$ on $R(0)$ is well evident. The early regime of relative dispersion is reported in Fig. 7. The value of the MLE $\lambda_L \simeq 0.6$ day^{-1} is on the same order as other estimates obtained in various ocean regions, as discussed later. The exponential growth has been adapted to the $R(0) \leq 5$ km curve, which has a fair compromise between having a sufficiently small initial separation and, at the same time, an acceptable pair statistics.

Relative diffusivity in the zonal and meridional directions, for initial separations $R(0) \leq 5$ km, is plotted in Fig. 8. Although the curves do not display a clean scaling behavior, in the time range of 10–100 days the diffusivities show some resemblance with the t^2 law expected in the Richardson dispersion regime. We will examine now the results obtained with scale-dependent indicators.

The FSLE has been evaluated for the same initial thresholds 1, 5, and 10 km; the results are reported in Fig. 9. Particle pairs are counted in the statistics if, at a given time, they happen to be separated by a distance smaller than the fixed threshold. The density of scales δ is fixed by setting $\rho = \sqrt{2}$. The maximum number of pairs considered varies with the initial threshold: 24 pairs for $R(0) \leq 1$ km, 30 pairs for $R(0) \leq 5$ km, and 39 pairs for $R(0) \leq 10$ km. Larger initial thresholds (viz., ≥ 100 km) could increase the statistics on the order of $\sim O(10)$, but we will not consider this opportunity because, with too large initial thresholds, mesoscale dispersion rates may be affected by the inhomogeneity of the flow. In other words, at a certain separation scale two drifters might be still spatially correlated in some regions of the domain but totally uncorrelated in some other ones, depending on the structure of the flow. The parameter ρ cannot be

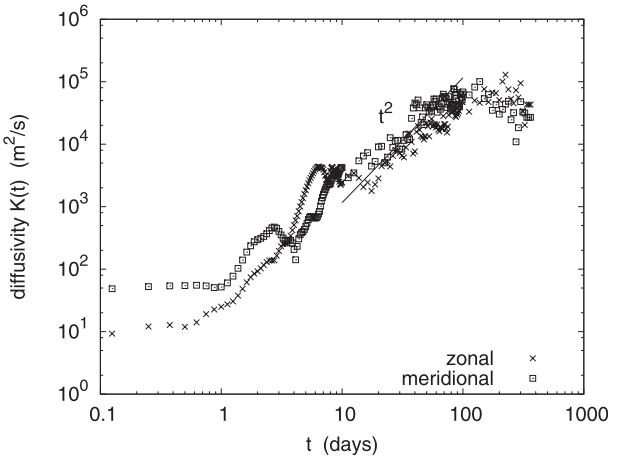


FIG. 8. Drifter relative diffusivity $K(t)$ in zonal and meridional components, for initial separations $R(0) \leq 5$ km. The t^2 scaling is plotted as reference to the Richardson regime. The time sampling is $\Delta t = 1/8$ day.

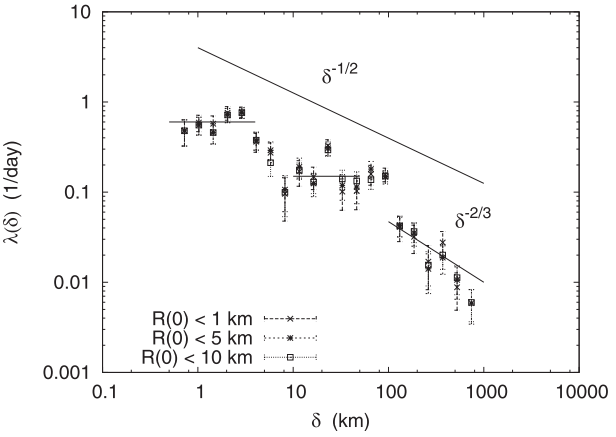


FIG. 9. FSLE for $R(0) \leq 1$, ≤ 5, and ≤ 10 km and amplification factor $\rho = \sqrt{2}$. The small-scale plateau corresponds to exponential separation with rate $\lambda_L \simeq 0.6$ day^{-1}. The $\sim\delta^{-2/3}$ scaling corresponds to the Richardson law. The $\delta^{-1/2}$ scaling corresponds to a k^{-2} spectrum. Error bars are the standard deviations of the mean values.

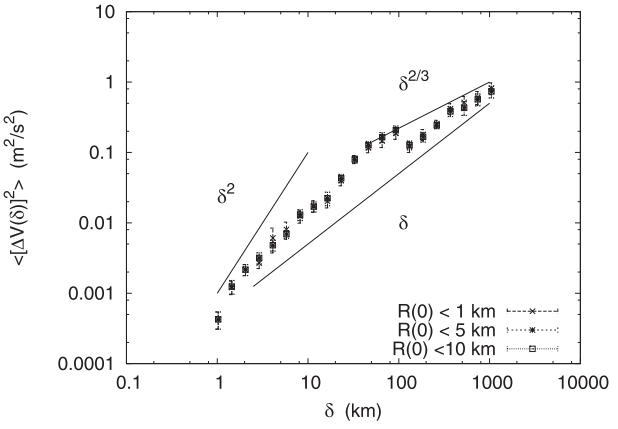


FIG. 10. FSRV computed together with the FSLE. The FSRV is the mean exit velocity of the distance between two drifters from the "shell" δ. The scalings δ^2, $\delta^{2/3}$, and δ correspond to k^{-3}, $k^{-5/3}$, and k^{-2} energy spectra, respectively. Error bars are the standard deviations of the mean values.

chosen arbitrarily close to 1 for obvious limitations because of finite resolution of the data. We have checked that, with $\rho = \sqrt{2}$, "clipping events" (i.e., suspect transitions between two neighboring scales in only one time step $\Delta t = 1/8$ days) are not significant. Taking a value $\delta_R \simeq 30$ km for the Rossby radius, we can see that mesoscale dispersion (scales $> \delta_R$) is compatible with a $\delta^{-2/3}$ Richardson regime, because it occurs in the inverse cascade range of QG turbulence. Cutoff due to finite lifetime of the trajectories occurs before reaching $\sim 10^3$ km separations. The range of 1–100 km is characterized by a step-like behavior of the FSLE. The first plateau in the submesoscale range $\sim O(1)$ km corresponds to exponential separation with $\lambda \simeq 0.6$ day^{-1}, in agreement with the result obtained before for $\langle R^2(t)\rangle$. The second plateau at $\simeq 0.15$ day^{-1} on $\sim O(\delta_R)$ scales is compatible with exponential separation due to a k^{-3} direct cascade of QG turbulence. It is unclear why there are two quasi-constant levels for $\lambda(\delta)$ that produce a significant variation of the exponential growth rate when δ decreases from mesoscale to submesoscale. Possible interpretations of this behavior may be found in the action of submesoscale vortices, even though the FSLE does not display a continuous cascade connecting these two scale ranges. The $\sim\delta^{-1/2}$ scaling is plotted as a reference to a k^{-2} energy spectrum. Another remark concerns the gap at $\delta \sim 100$ between the end of the plateau and the beginning of the $\sim\delta^{-2/3}$ regime. Inverse cascade implies that smaller eddies, formed by instability at the Rossby scale, tend to merge together in larger eddies up to scales in the range 10^2–10^3 km. Assuming this actually occurs, we also have to consider that the BC and BMC generate rings of size $\sim O(10^2)$ km that detach from the main currents. Such mesoscale rings can have trapping effects on the drifters, at least to some extent, which would determine an abrupt fall of the dispersion rate (FSLE). The presence of the BMC can also have a role in temporarily inhibiting the growth of the two-particle separation, until the drifters find their way eastward along the SAC.

Let us now consider the finite-scale (mean square) velocity difference (Fig. 10). The Lagrangian velocity components are reconstructed from the trajectories by means of a finite-difference scheme. We notice first that the FSRV returns back a slightly cleaner picture than other indicators. This may depend, for instance, on the fact that the amplification time of the separation between two drifters passing from δ to $\rho\delta$ is affected by large fluctuations due to the nonhomogeneous characteristics of the flow, whereas the (mean square) relative velocity at scale δ is less affected by the history of the dispersion between two scales. The two "valleys" at nearly 10 and 100 leave room to a hypothesis of trapping events by structures of size comparable with those scales. The FSRV is consistent with Richardson dispersion on scales larger than the Rossby radius (except for the valley at 100 km); with exponential separation for two subranges $\sim$(10–50) km and $\sim$1–5 km; and with a δ scaling in the subrange $\sim$(5–10) km, in turn consistent with a k^{-2} energy spectrum. The $\sim$(10–50)-km exponential regime can be associated to a k^{-3} direct cascade, whereas the $\sim$(81–5)-km exponential regime can be associated to the action of submesoscale vortices. From the FSRV, an "equivalent Lagrangian spectrum" $E_L(k) = \langle[\Delta V(k)]^2\rangle/k$ can be defined, by dimensional

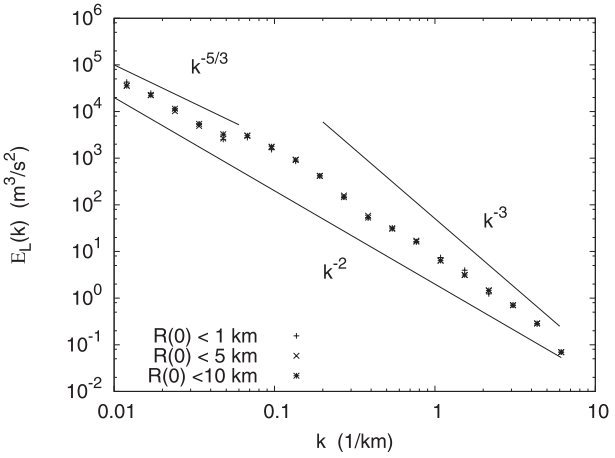


FIG. 11. Equivalent Lagrangian spectrum defined from the FSRV. The inverse cascade ($k^{-5/3}$), direct cascade (k^{-3}), and submesoscale (k^{-2}) spectra are plotted as reference. The Rossby radius $\simeq$ 30 km corresponds to a wavenumber $k \simeq 0.2$.

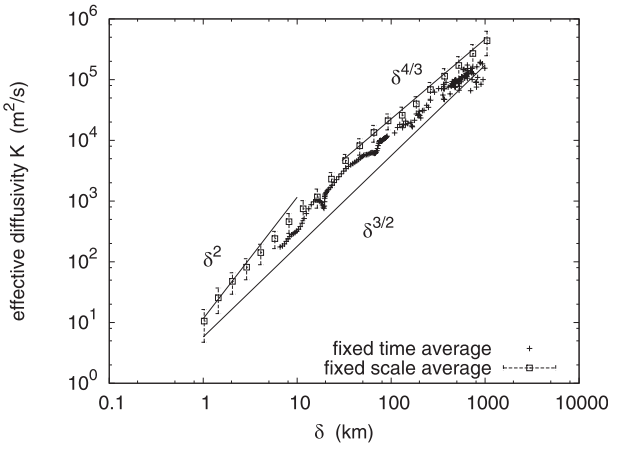


FIG. 12. Diffusivity as a function of the separation: fixed-time average $K(t)$ vs $\delta = \langle R^2(t)\rangle^{1/2}$ and fixed-scale average $K(\delta)$ vs δ. The $\delta^{4/3}$ and δ^2 correspond to $k^{-5/3}$ and k^{-3} spectra, respectively. The $\delta^{3/2}$ scaling corresponds to a k^{-2} spectrum.

arguments, replacing δ with $2\pi/k$ (Fig. 11). The same scenario formerly indicated by the FSRV is reproduced in k space by $E_L(k)$ as well.

We compare now the diffusivity (see Fig. 12) computed in both ways: as a fixed-time average (8) and as a fixed-scale average from the FSRV. Both quantities are plotted as functions of the separation between two drifters: $K(\delta) = (1/2)\delta\langle[\Delta V(\delta)]^2\rangle^{1/2}$, with δ as the independent variable, and $K(t)$ versus $\delta = \langle R^2(t)\rangle^{1/2}$, where the independent variable is the time t. The diffusivity is less affected by distortions present in the signal than other indicators. The two regimes $\sim\delta^{4/3}$ at the mesoscale and $\sim\delta^2$ at a scale $\sim O(\delta_R)$ are consistent with the inverse cascade $k^{-5/3}$ and direct cascade k^{-3}, respectively, as predicted by QG turbulence theory. A scaling $\sim\delta^{3/2}$, corresponding to a k^{-2} spectrum, connects scales on the order of the Rossby radius to the submesoscale, and a scaling $\sim\delta^2$ is the signature of exponential separation driven by velocity field features on scales $\sim O(1)$ km.

5. Numerical simulations

To check the consistency of the results obtained from the data analysis of the MONDO drifters, we have performed two numerical experiments in which $\sim O(10^2)$ virtual drifters are deployed in a surface current field generated by a global operational forecast system using the Hybrid Coordinates Ocean Model (HYCOM; Bleck and Benjamin 1993) and the Navy Coupled Ocean Data Assimilation (NCODA; Cummings 2005). The model grid step is $1/12°$ (approximately 7 km), and outputs are available with a 1-day time step. From the 32-layer global grid, the surface layer is extracted in the area within 45°–20°S and 60°–30°S for the same period of drifters trajectories (20 September 2007–21 October 2008). Conversion from Earth coordinates to meters is accomplished following the great circle distance approximation. The integration algorithm of the Lagrangian trajectories uses a fixed time step $\Delta t = 1/24$ day and trilinear interpolations. The maximum integration time is 400 days, but particles reaching the shoreline are stopped and removed from the subsequent integration.

We indicate the numerical experiments with E1 and E2. In the first one (E1), the drifters are uniformly deployed in an area of about 10×10 km^2 centered around a position corresponding to the mean initial location of MONDO drifters. The average initial distance between particle pairs is $\langle R(0)\rangle \simeq 5$ km. The lifetime of trajectories is between 150 and 200 days. In the second experiment (E2), the initial distribution of the drifters is characterized by larger separations: namely, comparable to the spacing of the numerical grid ($\sim$10 km). The average initial distance between particle pairs is $\langle R(0)\rangle \simeq 40$ km, and the duration of trajectories is 250–400 days.

Here, we present some comparisons between the analysis of data from model trajectories and those from the actual drifters, focusing on the relative dispersion process. First, we consider a fixed-time indicator [viz., relative dispersion $\langle R^2(t)\rangle$] for trajectories selected with small enough initial separation: that is, for $R(0) <$ 10 km. As can be seen in Fig. 13, the model outcome is in reasonable agreement with the behavior of actual drifters. In particular, experiment E1 is capable of

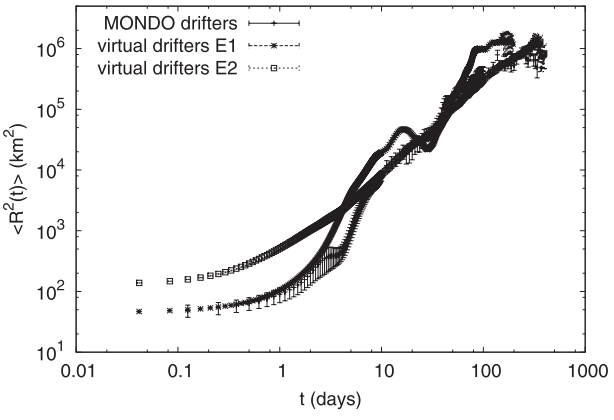


FIG. 13. Relative dispersion $\langle R^2(t)\rangle$ for initial separations $R(0) \leq$ 10 km for MONDO drifters and virtual drifters from numerical experiments E1 and E2. For virtual drifters, errors are on the order of point size; time sampling is $\Delta t = 1/8$ day for MONDO drifters and $\Delta t = 1/24$ day for virtual drifters.

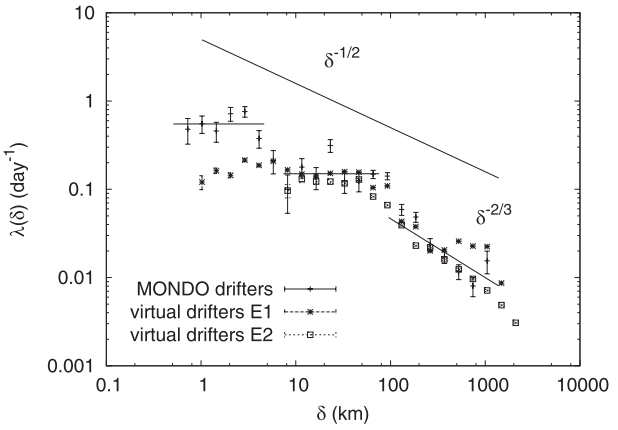


FIG. 14. FSLE for $R(0) \leq 50$ km and amplification factor $\rho = \sqrt{2}$ for MONDO drifters and virtual drifters from numerical experiments E1 and E2. For virtual drifters, errors are on the order of point size. The large-scale saturation (E1) depends on the value of the trajectory integration time.

reproducing the early growth of relative dispersion, but it cannot catch the late time behavior because of too short trajectories. On the other hand, with experiment E2 we obtain a nicer agreement at late times, thanks to the longer lifetime of virtual trajectories in this case, but we lose the agreement at early times because now the initial separation between particle pairs is on average much larger.

For what concerns fixed-scale indicators, we consider the FSLE and FSRV (Figs. 14, 15). To increase the statistics, we now select trajectories with a larger initial separation: that is, for $R(0) < 50$ km [similar results are found for smaller values of $R(0)$, though they are more noisy]. The behaviors of both FSLE and FSRV support a double-cascade scenario on the same scales as those found with MONDO drifters. The plateau value of FSLE at scales $O(\delta_R)$ is very close to the one found in the real experiment ($\lambda \simeq 0.15$ day^{-1}). At larger scales, for both numerical experiments E1 and E2, the behavior of FSLE is compatible with a scaling law $\lambda(\delta) \sim \delta^{-2/3}$ supporting an inverse energy cascade process. Experiment E2, which is characterized by longer trajectories, shows a clearer scaling, thanks to a larger number of pairs reaching this range of large scales. Mean-square velocity differences in the same range of scales display a reasonably clear $\delta^{2/3}$ scaling, also supporting an inverse energy cascade, with values close to those found with MONDO drifters. At separations smaller than the Rossby deformation radius, both indicators point to the presence of a direct enstrophy cascade: the FSLE is constant and the FSRV behaves as $\langle[\Delta V(\delta)]^2\rangle \sim \delta^2$. This only partially agrees with the results found for real drifters: namely, only in the scale range 10 km $< \delta <$ 50 km. At subgrid scales, velocity field features are not resolved and relative dispersion is necessarily a nonlocal exponential process driven by structures of size on the order of (at least) the Rossby radius. Correspondingly, the FSLE computed on model trajectories does not display the higher plateau level at scales smaller than 10 km.

Finally, the behavior of the relative diffusivity $K(\delta)$ as a function of the separation δ is shown in Fig. 16 for both MONDO and virtual drifters. Here, $K(\delta)$ is computed from the mean-square velocity difference, as described in sections 2c and 4b. Model and experimental data again are in agreement at scales larger than the numerical space resolution (~10 km). Indeed, in both numerical experiments E1 and E2, we find scaling behaviors compatible with a QG double cascade: $K(\delta) \sim \delta^{4/3}$ (corresponding to

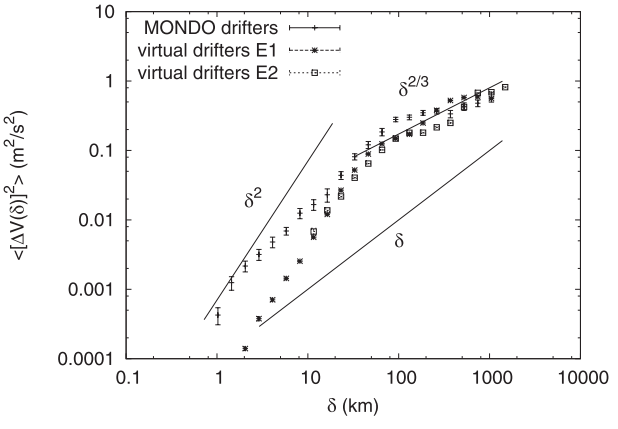


FIG. 15. FSRV for $R(0) \leq 50$ km for MONDO drifters and virtual drifters from numerical experiments E1 and E2. For virtual drifters, errors are on the order of point size.

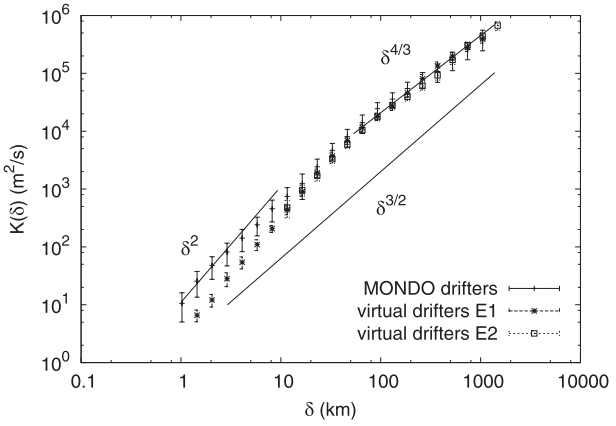


FIG. 16. Diffusivity $K(\delta)$ as function of the separation δ for MONDO drifters and virtual drifters from numerical experiments E1 and E2; here, $R(0) < 50$ km.

Richardson's superdiffusion in an inverse cascade regime) for $\delta > \delta_R$ and $K(\delta) \sim \delta^2$ (corresponding to a direct cascade smooth flow) for $\delta < \delta_R$. At variance with the outcome of the real experiment with MONDO drifters, here we are unable to detect any significant deviations from the QG turbulence scenario at small scales.

The failure of the model to reproduce flow features at very small scales is of course due to its finite spatial resolution, which is on the order of 10 km. Below this length scale, the velocity field computed in the model is smooth, whereas the one measured in the real ocean clearly displays active scales also in the range of 1–10 km. Nevertheless, the overall conclusion we can draw from the above comparisons is that the characteristics of the relative dispersion process found with MONDO drifters agree with those obtained with an ocean general circulation model (OGCM) for scales $\delta > 10$ km.

6. Discussion and conclusions

Lagrangian dispersion properties of drifters launched in the southwestern corner of the South Atlantic subtropical gyre have been analyzed through the computation of time-dependent and scale-dependent indicators.

The data come from a set of 39 WOCE–SVP drifters deployed in the Brazil Current around (24°S, 44°S) during the Monitoring by Ocean Drifters (MONDO) project, an oceanographic campaign planned by PROOCEANO and supported by Eni Oil do Brasil in relationship with an oil drilling operation. The experimental strategy of deploying part of the drifters in five-element clusters, with initial separation between drifters smaller than 1 km, allows us to study relative dispersion on a wide range of scales.

Single-particle analysis has been performed by computing classic quantities like Lagrangian autocorrelation functions and absolute dispersion, defined as the variance around the drifter mean position, as a function of the time lag from the release. Velocity variances ($\sim$500 cm^2 s^{-2}) and integral time scales ($\tau_L \sim 5$ days) are compatible with the estimates obtained in the analysis of the FGGE drifters (Figueroa and Olson 1989; Schäfer and Krauss 1995). Anisotropy of the flow is reflected in the different behavior of the zonal and meridional components of the absolute dispersion. Being the MONDO drifters advected mostly by the boundary currents surrounding the subtropical gyre, the Brazil Current first and the South Atlantic Current later, the meridional component of the absolute dispersion is dominant as long as the mean drifter direction is nearly southward (BC), whereas the zonal component dominates (see the appearance of the late ballistic regime) as the mean drifter direction is nearly eastward (SAC). Early time advection is modulated also by the response of the currents to a wind forcing of period $\sim$6.5 days, a characteristic meteorological feature of the BC dynamics.

Two-particle analysis has been performed by means of both fixed-time and fixed-scale averaged quantities. Classic indicators like the mean-square relative displacement and the relative diffusivities between two drifters as functions of the time lag from the release give loose information about early phase exponential separation, characterized by a mean rate $\lambda_L \simeq 0.6$ day^{-1}, and longtime dispersion approximated, to some extent, by Richardson superdiffusion before the cutoff due to the finite lifetime of the trajectories. Evidence of a small-scale exponential regime for relative dispersion is common to other drifter studies for different ocean regions (LaCasce and Ohlmann 2003; Ollitrault et al. 2005; Koszalka et al. 2009; Lumpkin and Elipot 2010). Scale-dependent indicators return back a cleaner picture, compatibly with the limited statistics allowed by the experimental data and the nonhomogeneous and nonstationary characteristics of the flow.

The FSLE displays a mesoscale (100–500 km) regime compatible with Richardson superdiffusion, with the Lagrangian counterpart of the 2D inverse cascade scenario characterized by a $k^{-5/3}$ energy spectrum. At scales smaller than 100 km, the FSLE has a step-like shape, with a first plateau at level $\sim$0.6 day^{-1} in the submesoscale range $\sim O(1)$ km and a second plateau at level $\simeq$0.15 day^{-1} for scales comparable with the Rossby radius of deformation ($\delta_R \simeq 30$ km). Constant FSLE in a range of scales corresponds to exponential separation. The $\sim O(\delta_R)$ plateau could be related to the 2D direct cascade characterized by a k^{-3} energy spectrum, whereas the origin of the $\sim O(1)$ km plateau is likely related to the existence of submesoscale features

of the velocity field, the role of which has been recently assessed by means of high-resolution 3D simulations of upper-ocean turbulence at Rossby numbers $R_o \sim O(1)$ (Capet et al. 2008a,b; Klein et al. 2008). The FSLE does not display a clean continuous cascade scaling $\sim\delta^{-1/2}$, corresponding to a k^{-2} energy spectrum, from subscales to mesoscales; however, it highlights the existence of scales of motion hardly reconcilable with the QG turbulence scenario, as analogously assessed also by Lumpkin and Elipot (2010) for drifter dispersion in the North Atlantic.

The FSRV measures the mean-square velocity difference at scale δ. The scaling of the FSRV is related to the turbulent characteristics of relative dispersion. The FSRV behavior is, under a certain point of view, cleaner than that of the FSLE, but it is affected by the presence of two ''valleys,'' roughly at $\simeq$10 and $\simeq$100 km, likely associated to trapping events (the same features are also present in the FSLE behavior). Coherent structures on scales $\sim$10 and $\sim$100 km may be responsible of the ''fall'' in the relative dispersion rate. These scales are on the order of the Rossby radius and of the mesoscale rings that detach from the current systems, respectively. We must also consider the role of the Brazil–Malvinas Confluence, which tends to inhibit the growth of the dispersion as the drifters, initially flowing southwestward along the Brazil Current, encounter the northeastward-flowing Malvinas Current before being eventually transported eastward along the South Atlantic Current. The FSRV displays a mesoscale $\sim\delta^{2/3}$ scaling (except for the valley), compatible with a $k^{-5/3}$ inverse cascade; a $\sim\delta^2$ scaling in the two subranges $\sim$(10–50) km and $\sim$(1–5) km, which corresponds to the step-like shape of the FSLE; and a $\sim\delta$ scaling which, to some extent, is compatible with a k^{-2} regime connecting scales on the order of the Rossby radius to the submesoscale (below which the velocity field becomes approximately smooth). The equivalent Lagrangian spectrum $E_L(k)$, formed by dividing the FSRV (essentially the relative kinetic energy at scale δ) by the wavenumber $k = 2\pi/\delta$, returns back the same scenario in k space.

Last, we have compared the scale-dependent relative diffusivity $K(\delta)$ constructed from the FSRV, for which δ is the independent variable, with the classic relative diffusivity $K(t)$ seen as a function of the mean separation between two drifters $\langle R^2(t)\rangle^{1/2}$, for which t is the independent variable. What emerges from the analysis of the diffusivities is that, in the mesoscale range, loosely from the Rossby radius up to scales $\sim O(10^2)$ km, $K(\delta) \sim \delta^{4/3}$, corresponding to the $k^{-5/3}$ inverse cascade; in the submesoscale range $\sim$1–5 km and in a limited subrange from about the Rossby radius down to $\sim$10 km, $K(\delta) \sim \delta^2$, corresponding to exponential separation; and, in the subrange $\sim$(5–10) km, the scaling $K(\delta) \sim \delta^{3/2}$ is compatible with a k^{-2} regime. The k^{-2} spectrum is a characteristic of upper-ocean turbulence when the Rossby number is on the order of $\sim O(1)$, as recently assessed with high-resolution 3D model simulations (Capet et al. 2008a,b; Klein et al. 2008), which connects the mesoscale to the submesoscale $\sim O(1–10)$ km (McWilliams 1985). Below the submesoscale, the velocity field is reasonably assumed to vary smoothly. A rough estimate of the Rossby number associated to the MONDO drifter dynamics gives a value (at least) $R_o = U/(Lf) \sim O(10^{-1})$, taking $U \sim 0.3$ m s^{-1}, $L \sim 30$ km, and $f \sim 10^{-4}$ s^{-1}, which is nonetheless considerably larger than the typical Rossby number in open ocean. Although the drifter data analysis does not show a clear evidence of a relative dispersion regime corresponding to the k^{-2} spectrum, the presence of velocity field features of size comparable to submesoscale vortices is reflected to some extent by the behavior of the small-scale relative dispersion process.

Numerical simulations of the Lagrangian dynamics have been performed with an OGCM of the South Atlantic (Huntley et al. 2010). The results concerning the relative dispersion essentially agree with the data analysis of the MONDO drifters, within the limits of the available numerical resolution. In particular, two-particle statistical indicators such as the FSLE, the FSRV, and the scale-dependent relative diffusivity $K(\delta)$, computed on the trajectories of virtual drifters, display the same behavior found for MONDO drifters for scales larger than approximately 10 km: that is, larger than the numerical grid spacing. Below this length scale, evidently, the model flow field is smooth; hence, relevant departures from QG turbulence and the role of submesoscale structures cannot be assessed. Further investigation on the modeling of submesoscale processes would be extremely useful to provide a clearer picture of the small-scale dynamics of the surface ocean circulation in the region.

Acknowledgments. FDS thanks Eni Oil do Brasil S.A. in the person of Ms. Tatiana Mafra for being the financial promoter of MONDO project and for making the experimental data available to the scientific community. SB acknowledges financial support from CNRS. We thank D. Iudicone and E. Zambianchi for useful discussion and suggestions. The authors are also grateful to three anonymous reviewers, who have helped to improve the substance and the form of this work with their critical remarks.

REFERENCES

Artale, V., G. Boffetta, A. Celani, M. Cencini, and A. Vulpiani, 1997: Dispersion of passive tracers in closed basins: Beyond the diffusion coefficient. *Phys. Fluids,* **9,** 3162–3171.

Assireu, A. T., 2003: Estudo das características cinemáticas e dinâmicas das águas de superfície do Atlântico Sul Ocidental a partir de derivadores rastreados por satélite. Ph.D. thesis, Instituto Nacional de Pesquisas Espaciais, 154 pp.

——, M. Stevenson, and J. Stech, 2003: Surface circulation and kinetic energy in the SW Atlantic obtained by drifters. *Cont. Shelf Res.,* **23,** 145–157.

Aurell, E., G. Boffetta, A. Crisanti, G. Paladin, and A. Vulpiani, 1996: Growth of non-infinitesimal perturbations in turbulence. *Phys. Rev. Lett.,* **77,** 1262–1265.

Batchelor, G. K., 1950: The application of the similarity theory of turbulence to atmospheric diffusion. *Quart. J. Roy. Meteor. Soc.,* **76,** 133–146.

Bleck, R., and S. Benjamin, 1993: Regional weather prediction with a model combining terrain-following and isentropic coordinates. Part I: Model description. *Mon. Wea. Rev.,* **121,** 1770–1785.

Boffetta, G., A. Celani, M. Cencini, G. Lacorata, and A. Vulpiani, 2000: Non-asymptotic properties of transport and mixing. *Chaos,* **10,** 50–60.

Bohr, T., M. H. Jensen, G. Paladin, and A. Vulpiani, 1998: *Dynamical Systems Approach to Turbulence*. Cambridge University Press, 350 pp.

Campos, E. J. D., J. L. Miller, T. J. Müller, and R. G. Peterson, 1995: Physical oceanography of the southwest Atlantic Ocean. *Oceanography,* **8,** 87–91.

Capet, X., J. C. McWilliams, M. J. Molemaker, and A. F. Shchepetkin, 2008a: Mesoscale to submesoscale transition in the California Current System. Part I: Flow structure, eddy flux, and observational tests. *J. Phys. Oceanogr.,* **38,** 29–43.

——, ——, ——, and ——, 2008b: Mesoscale to submesoscale transition in the California Current System. Part II: Frontal processes. *J. Phys. Oceanogr.,* **38,** 44–64.

Charney, J. G., 1971: Geostrophic turbulence. *J. Atmos. Sci.,* **28,** 1087–1094.

Cummings, J. A., 2005: Operational multivariate ocean data assimilation. *Quart. J. Roy. Meteor. Soc.,* **131,** 3583–3604.

de Castro, B. M., J. A. Lorenzetti, I. C. A. da Silveira, and L. B. de Miranda, 2006: Estrutura termohalina e circulaćão na região entre o Cabo de São Tomé (RJ) e o Chuí (RS). *O Ambiente Oceanográfico da Plataforma Continental e do Talude na Região Sudeste-Sul do Brasil,* C. L. D. B. Rossi-Wongtschowski and L. S.-P. Madureira, Eds., Edusp, 11–120.

Figueroa, H. A., and D. B. Olson, 1989: Lagrangian statistics in the South Atlantic as derived from SOS and FGGE drifters. *J. Mar. Res.,* **47,** 525–546.

Frisch, U., 1995: *Turbulence: The Legacy of A. N. Kolmogorov*. Cambridge University Press, 296 pp.

Garfield, N., 1990: The Brazil Current at subtropical latitudes. Ph.D. thesis, University of Rhode Island, 122 pp.

Gordon, A., and C. Greengrove, 1986: Geostrophic circulation of the Brazil-Falkland confluence. *Deep-Sea Res.,* **33A,** 573–585.

Hansen, D. V., and P. M. Poulain, 1996: Quality control and interpolations of WOCE–TOGA drifter data. *J. Atmos. Oceanic Technol.,* **13,** 900–909.

Houry, S., E. Dombrowsky, P. D. Mey, and J. Minster, 1987: Brunt-Väisälä frequency and Rossby radii in the South Atlantic. *J. Phys. Oceanogr.,* **17,** 1619–1626.

Huntley, H. S., B. L. Lipphardt Jr., and A. D. Kirwan Jr., 2010: Lagrangian predictability assessed in the East China Sea. *Ocean Modell.,* **36,** 163–178, doi:10.1016/j.ocemod.2010.11.001.

Klein, P., B. L. Hua, G. Lapeyre, X. Capet, S. L. Gentil, and H. Sasaki, 2008: Upper ocean turbulence from high-resolution 3D simulations. *J. Phys. Oceanogr.,* **38,** 1748–1763.

Koszalka, I., J. H. LaCasce, and K. A. Orvik, 2009: Relative dispersion in the Nordic Seas. *J. Mar. Res.,* **67,** 411–433.

Kraichnan, R. H., 1967: Inertial ranges in two-dimensional turbulence. *Phys. Fluids,* **10,** 1417–1423.

LaCasce, J. H., 2008: Statistics from Lagrangian observations. *Prog. Oceanogr.,* **77,** 1–29.

——, and C. Ohlmann, 2003: Relative dispersion at the surface of the Gulf of Mexico. *J. Mar. Res.,* **61,** 285–312.

Lacorata, G., E. Aurell, and A. Vulpiani, 2001: Drifter dispersion in the Adriatic Sea: Lagrangian data and chaotic model. *Ann. Geophys.,* **19,** 121–129.

——, ——, B. Legras, and A. Vulpiani, 2004: Evidence for a $k^{-5/3}$ spectrum from the EOLE Lagrangian balloons in the low stratosphere. *J. Atmos. Sci.,* **61,** 2936–2942.

Legeckis, R., and A. Gordon, 1982: Satellite observations of the Brazil and Falkland currents 1975 to 1976 and 1978. *Deep-Sea Res.,* **29,** 375–401.

Lentini, C., D. Olson, and G. Podestá, 2002: Statistics of Brazil Current rings observed from AVHRR: 1993 to 1998. *Geophys. Res. Lett.,* **29,** 1811.

Lima, I. D., C. A. E. Garcia, and O. O. Möller, 1996: Ocean surface processes on the southern Brazilian shelf: Characterization and seasonal variability. *Cont. Shelf Res.,* **16,** 1307–1317.

Lin, J. T., 1972: Relative dispersion in the enstrophy-cascading inertial range of homogeneous two-dimensional turbulence. *J. Atmos. Sci.,* **29,** 394–395.

Lumpkin, R., and S. Elipot, 2010: Surface drifter pair spreading in the North Atlantic. *J. Geophys. Res.,* **115,** C12017, doi:10.1029/2010JC006338.

McWilliams, J. C., 1985: Submesoscale, coherent vortices in the ocean. *Rev. Geophys.,* **23,** 165–182.

Müller, T. J., Y. Ikeda, N. Zangenberg, and L. V. Nonato, 1998: Direct measurements of western boundary currents off Brazil between 20°S and 28°S. *J. Geophys. Res.,* **103** (C3), 5429–5437.

Obhukov, A. M., 1941: Energy distribution in the spectrum of turbulent flow. *Izv. Akad. Nauk SSSR, Ser. Geofiz.,* **5,** 453–466.

Oliveira, L. R., A. R. Piola, M. M. Mata, and I. D. Soares, 2009: Brazil Current surface circulation and energetics observed from drifting buoys. *J. Geophys. Res.,* **114,** C10006, doi:10.1029/2008JC004900.

Ollitrault, M., C. Gabillet, and A. C. D. Verdiere, 2005: Open ocean regimes of relative dispersion. *J. Fluid Mech.,* **533,** 381–407.

Peterson, R. G., and L. Stramma, 1991: Upper-level circulation in the South Atlantic Ocean. *Prog. Oceanogr.,* **26,** 1–73.

Pezzi, L. P., R. B. Souza, M. S. Dourado, C. A. E. Garcia, M. M. Mata, and M. A. F. Silva-Dias, 2005: Ocean-atmosphere in situ observations at the Brazil-Malvinas Confluence region. *Geophys. Res. Lett.,* **32,** L22603, doi:10.1029/2005GL023866.

Piola, A. R., H. A. Figueroa, and A. A. Bianchi, 1987: Some aspects of the surface circulation south of 20°S revealed by first GARP global experiment drifters. *J. Geophys. Res.,* **92** (C5), 5101–5114.

——, O. O. Möller, R. A. Guerrero, and E. J. D. Campos, 2008: Variability of the subtropical shelf front off eastern South America: Winter 2003 and summer 2004. *Cont. Shelf Res.,* **28,** 1639–1648.

Richardson, L. F., 1926: Atmospheric diffusion shown on a distance-neighbor graph. *Proc. Roy. Soc. London,* **110A,** 709–737.

Schäfer, H., and W. Krauss, 1995: Eddy statistics in the South Atlantic as derived from drifters drogued at 100 m. *J. Mar. Res.,* **53,** 403–431.

Stech, J., and J. Lorenzetti, 1992: The response of the South Brazil Bight to the passage of wintertime cold fronts. *J. Geophys. Res.,* **97** (C6), 9507–9520.

Stevenson, M. R., 1996: Recirculation of the Brazil Current south of 23°S. *WOCE International Newsletter,* No. 22, WOCE International Project Office, Southampton, United Kingdom, 30–32.

Stramma, L., and M. England, 1999: On the water masses and mean circulation of the South Atlantic Ocean. *J. Geophys. Res.,* **104** (C9), 20 863–20 883.

Sybrandy, A. L., and P. P. Niiler, 1991: WOCE/TOGA SVP Lagrangian drifter construction manual. Scripps Institution of Oceanography Rep. 91/6, 58 pp.

Taylor, G. I., 1921: Diffusion by continuous movements. *Proc. London Math. Soc.,* **20,** 196–212.

Thomas, L. N., A. Tandon, and A. Mahadevan, 2008: Submesoscale processes and dynamics. *Eddy Resolving Ocean Modeling,* M. W. Hecht and H. Hasumi, Eds., Amer. Geophys. Union, 17–38.